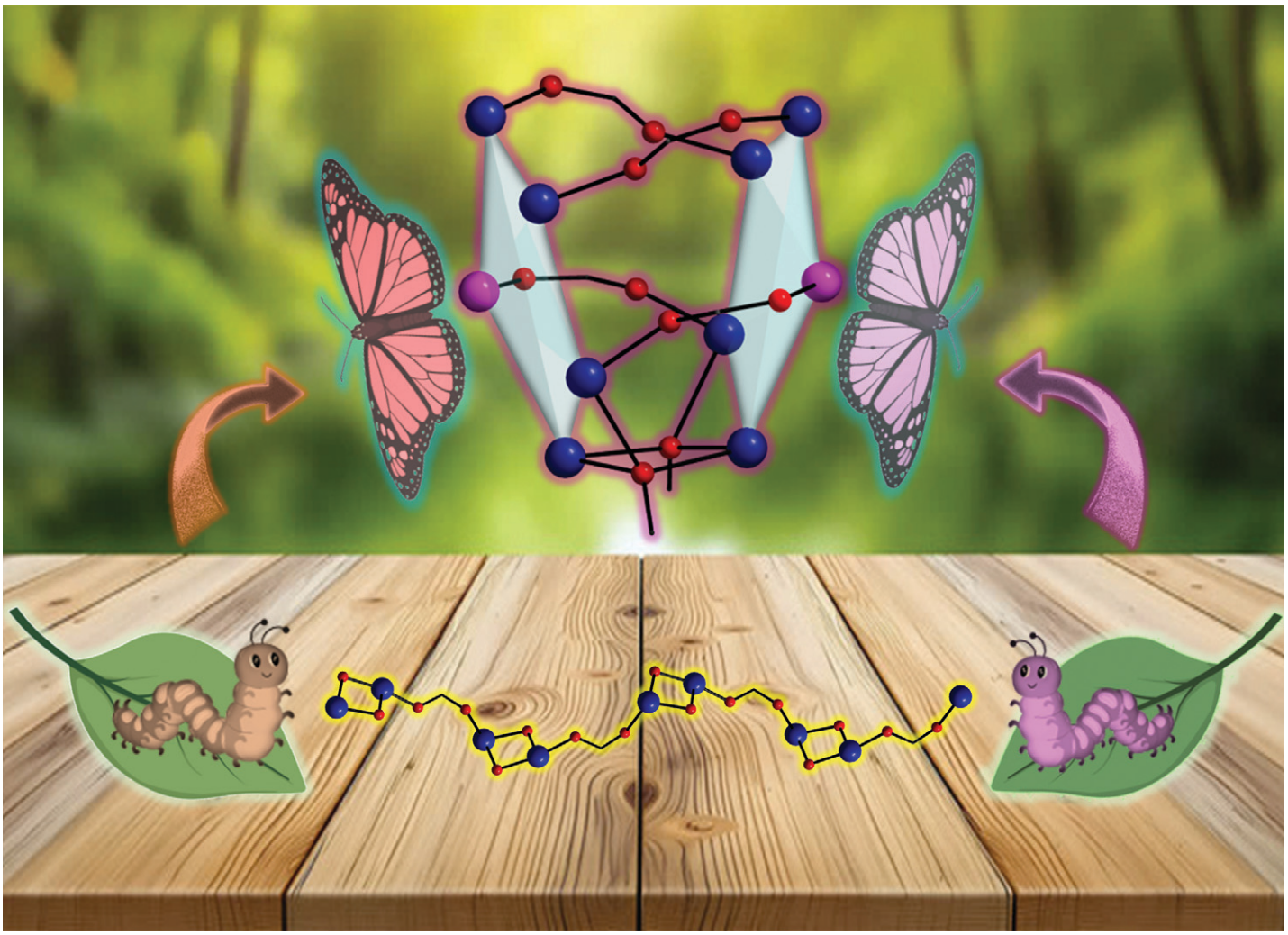

Showcasing research from Professor Theocharis C. Stamatatos laboratory, Department of Chemistry, University of Patras, Patras, Greece.

A preformed 1-D $\{CuII2\}_n$ helical chain as precursor to a decanuclear 0-D $\{CuII8MnII2\}$ cluster: synthesis, structure and magnetism

This work explores the coordination chemistry of the Schiff base ligand *N*-salicylidene-2-amino-5-chlorobenzoic acid in homo- and heterometallic systems. A one-dimensional Cu^{II} helical chain and a rare decanuclear Cu^{II}/Mn^{II} cluster are synthesized and structurally characterized. The study reveals an unusual $\{Cu_8Mn_2\}$ core and provides insight into templated cluster assembly. Magnetic measurements uncover dominant antiferromagnetic interactions, highlighting preformed metal assemblies as versatile building blocks for unprecedented heterometallic architectures.

As featured in:

See Theocharis C. Stamatato *et al.*, *CrystEngComm*, 2026, **28**, 112.

ROYAL SOCIETY OF CHEMISTRY

rsc.li/crystengcomm

Registered charity number: 207890

CrystEngComm

PAPER

View Article Online
View Journal | View Issue

Cite this: *CrystEngComm*, 2026, **28**, 112

A preformed 1-D $\{Cu^{II}_2\}_n$ helical chain as precursor to a decanuclear 0-D $\{Cu^{II}_8Mn^{II}_2\}$ cluster: synthesis, structure and magnetism

Konstantinos N. Pantelis,[a] Dimitris I. Alexandropoulos,*[a] Albert Escuer,[b] George E. Kostakis *[c] and Theocharis C. Stamatatos *[ad]

Received 22nd November 2025,
Accepted 10th December 2025

DOI: 10.1039/d5ce01110h

rsc.li/crystengcomm

The Schiff base ligand, *N*-salicylidene-2-amino-5-chlorobenzoic acid ($sacbH_2$), was initially employed in both homometallic Cu^{II} and heterometallic Mn^{II}/Cu^{II} coordination chemistry. A 1-D helical chain, $[Cu^{II}_2(sacb)_2(MeOH)]_n$ (**1**), and a decanuclear 0-D heterometallic cluster, $[Cu^{II}_8Mn^{II}_2(OH)_4(sacb)_8(H_2O)_2]$ (**2**), were synthesized and fully characterized. Complex **2** is one of the two highest nuclearity Mn^{II}/Cu^{II} complexes reported to date and exhibits a unique $\{Cu_8Mn_2(\mu_3\text{-}OH)_4(\mu\text{-}OR)_6(\mu_3\text{-}OR)_2(\mu\text{-}O_2CR)_2\}^{6+}$ core composed of two oppositely oriented pentanuclear $\{Cu_4Mn\}$ units, each featuring two vertex-sharing $\{Cu_2Mn\}$ triangles. The presence of the $\{Cu_2(sacb)_2\}$ fragment in both species suggests a templating role of the preformed chain **1** in the assembly of molecular cluster **2**. Variable-temperature dc magnetic susceptibility studies reveal predominant antiferromagnetic interactions between $Cu^{II}\cdots Mn^{II}$ and $Cu^{II}\cdots Cu^{II}$ centers, with exchange coupling constants: J_1 = −16.5(1) cm^{-1}, J_2 = −35.1(5) cm^{-1} and J_3 = +0.7(3) cm^{-1}. These findings highlight the utility of preformed oligonuclear and polymeric 3d-metal species as building blocks for the preparation of heterometallic 3d/3d′ polynuclear complexes with novel architectures and tailored physicochemical properties.

1. Introduction

The synthesis of high nuclearity 0-D coordination clusters from paramagnetic first row transition metal ions remains a central objective in molecular inorganic chemistry, motivated by applications in catalysis, bioinorganic chemistry, molecule-based magnetism and optics.[1] Structurally, many such aggregates resemble structural motifs found in extended solids, such as perovskites, brucites and supertetrahedra, build through rich arrays of oxo/hydroxo and carboxylate bridges that enable predictable connectivity and robust cores.[2] In molecular magnetism, polynuclear 3d systems that combine large spin ground states with significant axial anisotropy can display slow relaxation of the magnetization and magnetic hysteresis and act as single molecule magnets (SMMs), offering a bottom up route to nanoscale information storage and spin based devices.[3,4] Historically, SMM research has been dominated by manganese chemistry, especially mixed valence species rich in Mn^{III} ions, where cooperative alignment of Jahn–Teller axes within approximately octahedral crystal fields enhances anisotropy and leads to large effective energy barriers (U_{eff}) for the magnetization reversal.[5,6]

Heterometallic cluster chemistry opens up more design options. Combining two distinct 3d (or 3d/4f) ions in the same molecule allows tuning of exchange pathways, balancing of ferro- and antiferromagnetic interactions, and access to metal topologies that are rare in homometallic systems.[7,8] Despite clear benefits, 3d/3d′ systems still lag behind 3d/4f in range and variety, reflecting synthetic challenges and the need for ligands that support multiple bridging modes while remaining compatible with two different metal ions.[8] Within this context, Mn^{II}/Cu^{II} clusters are particularly attractive and comparatively underexplored.[9,10] High-spin Mn^{II} ion (d^5, $^6A_{1g}$ in O_h symmetry) is often magnetically isotropic but can exhibit field-induced slow relaxation when its coordination environment and local anisotropy are judiciously tuned, making it a useful probe of structure–property relationships.[9g,h,11] Cu^{II} ion, by contrast, is geometry labile owing to Jahn–Teller distortion, typically resulting in axially elongated octahedral environments and enabling diverse superexchange pathways that are highly sensitive to small structural perturbations. Oligo- and polynuclear Cu^{II}

[a] *Department of Chemistry, University of Patras, Patras 26504, Greece. E-mail: thstama@upatras.gr*
[b] *Departament de Química Inorgànica i Orgànica, Secció de Química Inorgànica, Institut de Nanociència i Nanotecnologia (IN2UB), Universitat de Barcelona, Martí i Franquès 1-11, 08028 Barcelona, Spain*
[c] *Department of Chemistry, School of Life Sciences, University of Sussex, Brighton BN1 9QJ, UK*
[d] *Foundation for Research and Technology – Hellas (FORTH/ICE-HT), Institute of Chemical Engineering Sciences, Platani, P.O. Box 1414, Patras 26504, Greece*

complexes have therefore served as reference systems for magnetostructural correlations and EPR parameter benchmarking, and they remain excellent partners for constructing heterometallic Mn^{II}/Cu^{II} clusters.[12]

Two complementary synthetic strategies are commonly employed to access 3d/3d′ aggregates. The first is one-pot self-assembly from mixed metal salts and a suitable polydentate, bridging/chelating ligand.[8,10] The second is more targeted and involves reactions of preformed 3d building blocks with a second 3d′ source to guide aggregation around a preorganized fragment. This targeted approach reduces the combinatorial complexity of solution self-assembly but still requires judicious selection of polydentate organic ligand and attention to the coordination flexibility of Cu^{II}.[9c,13] Our research has focused on Schiff base ligands, particularly *N*-salicylidene-2-amino-5-chlorobenzoic acid ($sacbH_2$), which, upon complete deprotonation, can act as a tetradentate (O_3N) chelating and bridging ligand (Fig. 1). $SacbH_2$ has already proven versatile in homometallic 3d, 4f and 3d/4f cluster chemistry, including species with notable SMM behavior.[14] However, it has not been used in 3d/3d′ heterometallic cluster chemistry; only a handful of related ligands have appeared in Zn^{II}/Fe^{III} or Zn^{II}/Cr^{III} systems.[15] This gap motivated the use of $sacbH_2$ as a ligand in Mn^{II}/Cu^{II} cluster chemistry.

Herein we report the first Mn^{II}/Cu^{II} cluster derived from the use of $sacbH_2$ ligand using the building block synthetic approach. A preformed one-dimensional (1-D) Cu^{II} helical coordination polymer, $[Cu^{II}_2(sacb)_2(MeOH)]_n$ (**1**), obtained in high yield, was combined in a one-pot reaction with a Mn^{II} source to produce the decanuclear 0-D heterometallic cluster $[Cu^{II}_8Mn^{II}_2(OH)_4(sacb)_8(H_2O)_2]$ (**2**), in similarly high yield. Complex **2** features a metal core that comprises two oppositely oriented {Cu_4Mn} subunits, each built from two vertex-sharing {Cu_2Mn} triangles and linked by ligands' phenoxo and carboxylate bridges. To our knowledge, this metal topology is unprecedented among 3d/3d′ clusters and, together with the decanuclear wheel-like $[Cu_5Mn_5(edpba)_5(dmso)_7(H_2O)_7]$ complex, containing the *N*,*N*′-2,2′-ethylenediphenylenebis(oxamic acid) ligand,[9a] represents the highest nuclearity reported for discrete Mn^{II}/Cu^{II} clusters to date. The chemical and structural identities of both complexes **1** and **2** were confirmed by single-crystal X-ray diffraction, elemental (C, H, N) analysis, and IR spectroscopy. Additionally, magnetic studies on complex **2** revealed predominant antiferromagnetic interactions between the metal centers, leading to a small – if not zero – spin ground state.

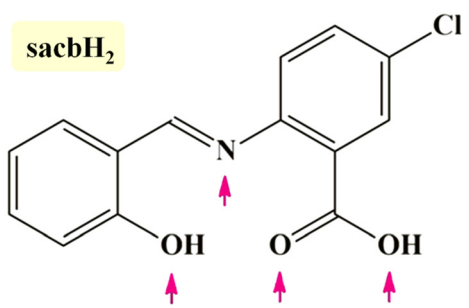

Fig. 1 Structural formula and abbreviation of the Schiff base ligand *N*-salicylidene-2-amino-5-chlorobenzoic acid ($sacbH_2$) employed in this work. The arrows highlight the potential donor atoms.

2. Experimental section

a. Materials, physical and spectroscopic measurements

All manipulations were performed under aerobic conditions using materials (reagent grade) and solvents as received unless otherwise noted. The Schiff base ligand $sacbH_2$ was prepared, purified, and characterized as described elsewhere.[14a,d] Elemental analyses (C, H, and N) were performed by the University of Patras microanalytical service. Infrared (IR) spectra (4000–400 cm^{-1}) were recorded in the solid state using a Perkin-Elmer 16 PC spectrometer with samples prepared as KBr pellets. Direct current (dc) magnetic susceptibility studies for compound **2** were performed at the Scientific and Technological Center University of Barcelona (CCiT-UB) on a DSM5 Quantum Design magnetometer. Diamagnetic corrections were applied to the observed paramagnetic susceptibility using Pascal's constants.[16]

b. Synthesis of $[Cu_2(sacb)_2(MeOH)]_n$ (1)

To a stirred, yellow solution of $sacbH_2$ (0.06 g, 0.20 mmol) and NEt_3 (56 μL, 0.40 mmol) in solvent MeOH (10 mL) was added solid $Cu(ClO_4)_2{\cdot}6H_2O$ (0.04 g, 0.10 mmol). The resulting dark green slurry was stirred for 20 min, during which time the entire $Cu(ClO_4)_2{\cdot}6H_2O$ solid dissolved and the color of the solution remained dark green. The solution was then filtered, and the filtrate was allowed to evaporate slowly at room temperature. After one day, X-ray quality well-formed brown block-shaped crystals of **1** appeared, and these were collected by filtration and washed with cold MeOH (2 × 2 mL) and Et_2O (2 × 5 mL). The yield was 92% (based on the organic chelate available). Upon dryness (in air) the crystalline solid was analyzed as **1**. Anal. calc. for $C_{29}Cl_2H_{20}N_2O_7Cu_2$ (found values in parentheses): C 49.30 (49.41), H 2.85 (2.94) and N 3.97 (3.88) %. Selected IR data (KBr, cm^{-1}): 1631 (s), 1606 (s), 1545 (m), 1467 (m), 1438 (m), 1406 (m), 1340 (m), 1282 (m), 1227 (w), 1178 (m), 1154 (w) 1118 (m), 1031 (m), 972 (w), 898 (m), 849 (m), 796 (m), 744 (s), 709 (w), 636 (w), 598 (w), 571 (m), 548 (w), 500 (w), 463 (w), 438 (w).

c. Synthesis of $[Cu_8Mn_2(OH)_4(sacb)_8(H_2O)_2]$ (2)

To a stirred, dark green slurry of **1** (0.07 g, 0.10 mmol) in MeCN (15 mL) was added solid $Mn(O_2CMe)_2{\cdot}4H_2O$ (0.05 g, 0.20 mmol). The resulting green-brown suspension was refluxed for 2 h, during which time all solids dissolved, and the color of the solution remained green-brown. The solution was then filtered, and the filtrate was allowed to evaporate slowly at room temperature. After three days, X-ray quality well-formed green plate-shaped crystals of

2·3.33MeCN appeared, and these were collected by filtration and washed with cold MeCN (2 × 2 mL) and Et_2O (2 × 5 mL). The yield was 58% (based on the organic chelate available). Upon dryness in air, the crystalline solid was analyzed as lattice solvate-free **2**. Anal. calc. for $C_{112}Cl_8H_{72}N_8O_{30}Cu_8Mn_2$ (found values in parentheses): C 46.20 (46.14), H 2.49 (2.56) and N 3.85 (3.73) %. Selected IR data (KBr, cm^{-1}): 1605 (s), 1589 (s), 1540 (w), 1462 (m), 1442 (m), 1413 (w), 1366 (w), 1305 (w), 1248 (w), 1183 (m), 1152 (m) 1120 (m), 1029 (w), 983 (w), 900 (w), 849 (w), 823 (w), 797 (w), 758 (w), 742 (w), 666 (w), 559 (w).

d. Single-crystal X-ray crystallography

Brown single crystals of complex **1** (0.18 × 0.16 × 0.10 mm) and green single crystals of complex **2** (0.12 × 0.10 × 0.02 mm) were mounted onto a cryoloop using adequate inert oil,[17] and immediately cooled at 102(4) K (for **1**) and 100 K (for **2**). X-ray diffraction data were collected for **1** using a Xcalibur, Eos, Gemini ultra diffractometer and utilizing CuKα monochromated radiation (λ = 1.54184 Å). Considering complex **2**, X-ray diffraction data were collected on a XtaLAB AFC11 (RCD3) quarter-chi single diffractometer and utilizing CuKα monochromated radiation (λ = 1.54184 Å). All structures were solved using the charge-flipping algorithm, as implemented in the program SUPERFLIP,[18] and refined by full-matrix least-squares techniques against F^2 using the SHELXL[19] program through the OLEX2 interface.[20] The non-hydrogen atoms were successfully refined using anisotropic displacement parameters, and hydrogen atoms bonded to the carbon atoms of the ligands and those of the hydroxido groups were placed at their idealized positions using appropriate HFIX instructions in SHELXL. All H atoms were either located by different maps and refined isotropically or they were introduced at calculated positions as riding on their respective bonded atoms. The asymmetric unit of **2** contains one and a half decanuclear cluster compounds as well as five MeCN solvate molecules of crystallization. Various figures of both structures were created, using Diamond 3[21] and Mercury[22] software packages. The unit cell parameters, structure solution, and refinement details of compounds **1** and **2** are summarized in Table S1. Further crystallographic details of **1** and **2** can be found in the corresponding CIF files provided in the SI.

3. Results and discussion

a. Synthetic comments and IR spectra

Copper(II) complexes containing organic chelating ligands are known for their high thermodynamic stability, making them excellent precursors for the development of novel compounds with unique structures and interesting magnetic, catalytic and biological properties.[9c,13] Accordingly, the reaction of $Cu(ClO_4)_2{\cdot}6H_2O$ with $sacbH_2$ and NEt_3 in a 1 : 2 : 4 molar ratio in solvent MeOH led to the formation of a brown crystalline one-dimensional helical chain, $[Cu^{II}_2(sacb)_2(MeOH)]_n$ (**1**), in high yield (~92%). The general formation of **1** is summarized by the following stoichiometric eqn (1):

$$\begin{gathered}2n\ Cu(ClO_4)_2{\cdot}6H_2O + 2n\ sacbH_2 + 4n\ NEt_3 + n\ MeOH \\ \downarrow MeOH \\ [Cu^{II}_2(sacb)_2(MeOH)]_n + 4n\ (NHEt_3)(ClO_4) + 12n\ H_2O\end{gathered} \quad (1)$$

The $sacbH_2$-to-NEt_3 molar ratio of 2 : 4 (*viz.* 1 : 2) has ensured the complete deprotonation of the organic chelate, while the choice of the MeOH was proved essential for the high yield synthesis, crystallinity and purity of the 1-D polymer **1**. Reactions in alternative solvent media have not afforded any crystalline products.

Given that $sacbH_2$ has not been previously employed in heterometallic 3d/3d′ chemistry, various heterometallic reactions were investigated. This study specifically targeted the use of Cu^{II} and Mn^{II} as the 3d-metal ions. Notably, the self-assembly reaction between the coordination polymer **1** and $Mn(O_2CMe)_2{\cdot}4H_2O$ in a 1 : 2 molar ratio in MeCN under refluxing conditions produced a green-brown solution. From this, green crystals of the decanuclear cluster $[Cu^{II}_8Mn^{II}_2(OH)_4(sacb)_8(H_2O)_2]$ (**2**) were isolated in good yield (~58%). The general formation of complex **2** is summarized by the following stoichiometric eqn (2).

$$\begin{gathered}4\ [Cu^{II}_2(sacb)_2(MeOH)]_n + 2n\ Mn(O_2CMe)_2{\cdot}4H_2O \\ \downarrow MeCN \\ n\ [Cu^{II}_8Mn^{II}_2(OH)_4(sacb)_8(H_2O)_2] + 4n\ MeCO_2H + 4n\ MeOH + 2n\ H_2O\end{gathered} \quad (2)$$

Complexes **1** and **2** are air- and moisture-stable crystalline solids at room temperature. Importantly, we were unable to isolate compound **2** through 'one-pot' reactions between $Cu(ClO_4)_2{\cdot}6H_2O$, $Mn(O_2CMe)_2{\cdot}4H_2O$ and $sacbH_2$, despite utilizing various solvents, experimental conditions, and external bases (organic or inorganic). This suggests that heterometallic complex **2** can only be obtained in a pure, crystalline form by using the 1-D polymer **1** as a precursor and $Mn(O_2CMe)_2{\cdot}4H_2O$ as the Mn^{II} source. The acetate ions from the Mn^{II} salt likely play a key role in facilitating the formation of OH^- bridges *via* deprotonation of water molecules present in solution (either from the MeCN solvent or from the $Mn(O_2CMe)_2{\cdot}4H_2O$ starting material).

The choice of the reaction solvent is critical for both the formation and crystallization of complex **2**. In the absence of MeCN, no heterometallic product could be isolated. Instead, either the homometallic polymer **1** formed, or non-crystalline, oily/amorphous materials were obtained that could not be further characterized. Additionally, when the 2 : 1 stoichiometric reaction

between **1** and $Mn(O_2CMe)_2{\cdot}4H_2O$ was carried out, only green microcrystalline solids were produced rather than single crystals. These solids were confirmed as complex **2** through IR spectroscopy and elemental analysis (C, H, N).

The IR spectra of $sacbH_2$ ligand and complexes **1** and **2** are presented in Fig. S1. The presence of coordinated MeOH group in **1**, and H_2O groups and OH^- bridging ligands in **2**, is confirmed by the weak broad bands at 3369 cm^{-1} and 3419 cm^{-1}, respectively. Several medium-intensity bands for both compounds in the ~1545–1248 cm^{-1} range are assigned to contributions from the stretching vibrations of the aromatic rings of $sacb^{2-}$, while the strong bands at ~1606 cm^{-1} correspond to the ν(C═N) vibration of $sacb^{2-}$. These bands are shifted to lower frequency relative to the free ligand $sacbH_2$ [ν(C═N) = 1613 cm^{-1}], consistent with coordination of the imino N atom to the metal centers.[23]

b. Description of structures

The coordination polymer **1** crystallizes in the orthorhombic $P2_12_12_1$ space group and is crystal lattice solvate-free, while the decanuclear cluster **2** crystallizes in the monoclinic $C2/c$ space group with two crystallographically independent cluster molecules and ten MeCN molecules of crystallization per three decanuclear clusters; the latter will not be further discussed. Thus, only the one decanuclear moiety will be discussed in detail as a representative example. Selected interatomic distances and angles for **1** and **2** are listed in Tables S2 and S3, respectively. The oxidation states of the Mn ions present in **2** were confirmed by charge balance considerations and bond valence sum (BVS) calculations (Table S4).[24] As a result, the Mn ions were assigned to the 2+ oxidation state.

The repeating unit of the 1-D polymer **1**, $[Cu^{II}_2(sacb)_2(MeOH)]_n$, is depicted in Fig. 2a. Within this structure, two Cu^{II} ions are bridged by the phenoxo groups (O3, O6) from two doubly deprotonated $sacb^{2-}$ ligands, forming a $\{Cu_2(\mu\text{-}OR)_2\}^{2+}$ core, as illustrated in Fig. 2b (Cu1···Cu2 = 3.036(1) Å, Cu1–O3–Cu2 = 101.1(2)° and Cu1–O6–Cu2 = 100.6(2)°). The $\{Cu_2(\mu\text{-}OR)_2\}^{2+}$ diamond-like core is not strictly planar and the deviation of all atoms from the best-mean-plane of Cu1–O6–Cu2–O3 is 0.077 Å; the Cu^{II} atoms are located above and the O atoms below the mean plane. The two tetradentate $sacb^{2-}$ ligands exhibit different coordination modes; $\eta^2{:}\eta^1{:}\eta^1{:}\mu$ and $\eta^2{:}\eta^1{:}\eta^1{:}\eta^1{:}\mu_3$. These chelating ligands coordinate to the Cu1 and Cu2 centers, respectively, through their phenoxo-O, imino-N, and carboxylate-O atoms (Fig. 2c). Additionally, the latter ligand bridges to the Cu1 atom of an adjacent $\{Cu_2\}$ unit *via* its carboxylate O2 atom in an *anti*-fashion, highlighted by yellow dashed lines in Fig. 2a. This linkage is infinitely repeated to yield a 1-D, helical chain (Cu1···Cu2···Cu1 angle = 140.29°) that runs parallel to the *a*-axis (Fig. 3). The coordination sphere of the Cu2 ion is completed by a terminal MeOH solvate molecule, coordinated through the O41 atom. This MeOH molecule is H-bonded to the carboxylate O2 atom of a $sacb^{2-}$ group from an adjacent $\{Cu_2\}$ unit; the dimensions of this

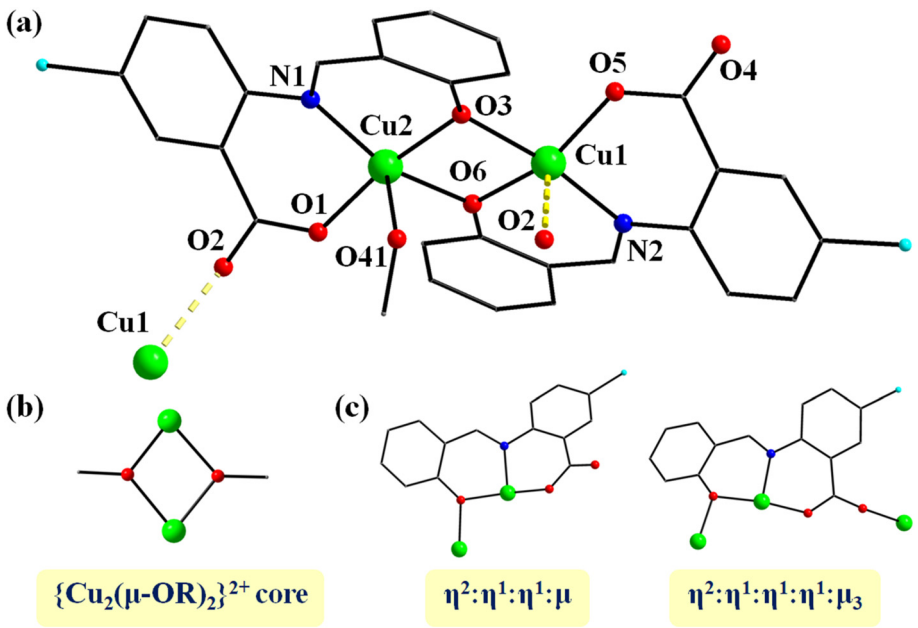

Fig. 2 (a) Partially labeled representation of the $\{Cu_2(sacb)_2(MeOH)\}$ repeating unit of the 1-D polymer **1**. The yellow dashed lines indicate the carboxylate O2 atoms, which are responsible for the polymerization of the dinuclear repeating units. (b) The $\{Cu_2(\mu\text{-}OR)_2\}^{2+}$ core of **1**. (c) The crystallographically established coordination modes of $sacb^{2-}$ ligands in **1**. All H atoms are omitted for clarity. Color scheme: Cu^{II}, green; O, red; N, blue; C, gray; Cl, cyan.

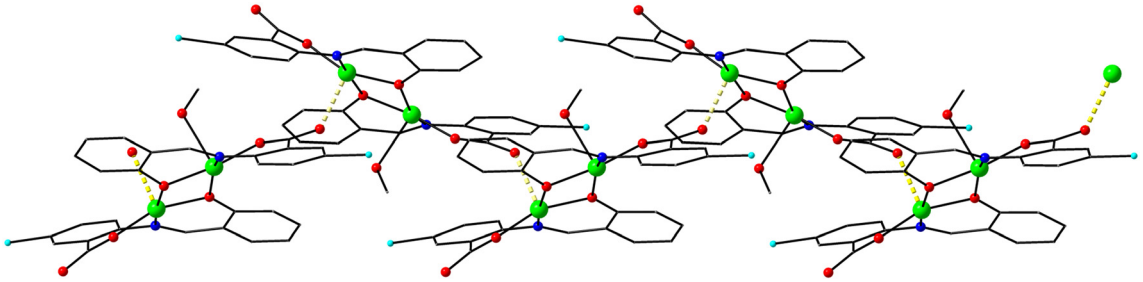

Fig. 3 Representation, along the crystallographic *a*-axis, of a section of the 1-D chain of **1**, showing the alternating $\{Cu_2(sacb)_2(MeOH)\}$ repeating units connected to each other through the $Cu–O_{carboxylate}$ bonds (yellow dashed lines). All H atoms are omitted for clarity. Color scheme: Cu^{II}, green; O, red; N, blue; C, gray; Cl, cyan.

H-bonding interaction are: O41···O2 = 2.732 Å, H41···O2 = 1.976 Å, and O41–H41···O2 = 140.9°.

The Cu1 and Cu2 ions are five-coordinate with distorted square pyramidal geometries. This is confirmed by the shape-determining bond angle analysis using the Reedijk and Addison approach,[25] which yields average trigonality index (τ) values of 0.26 for Cu1 and 0.20 for Cu2, where τ values range from 0 (for ideal square pyramidal geometry) to 1 (for ideal trigonal bipyramidal geometry). The equatorial planes of the Cu^{II} square pyramidal geometries are occupied by two O,N-donor atoms (O5, N2 for Cu1/O1, N1 for Cu2) and two bridging phenoxo-O atoms (O3, O6) of $sacb^{2-}$. In the axial positions, Cu1 is coordinated to the carboxylate O2 atom from a $sacb^{2-}$ ligand that belongs to a neighboring $\{Cu_2\}$ unit, while Cu2 is coordinated to the O41 atom of the terminal MeOH solvate molecule.

The Cu1···Cu2 distance between the $\{Cu_2\}$ repeating units of the 1-D chain is ~5.8 Å, while the shortest Cu···Cu separation between the chains (Fig. S2) is ~7.5 Å, and no significant inter-chain H bonding or π–π stacking interactions appear to affect the structural isolation of the 1-D polymer.

The molecular structure of one of the two crystallographically independent $[Cu_8Mn_2(OH)_4(sacb)_8(H_2O)_2]$ (**2**) clusters is depicted in Fig. 4a, and the

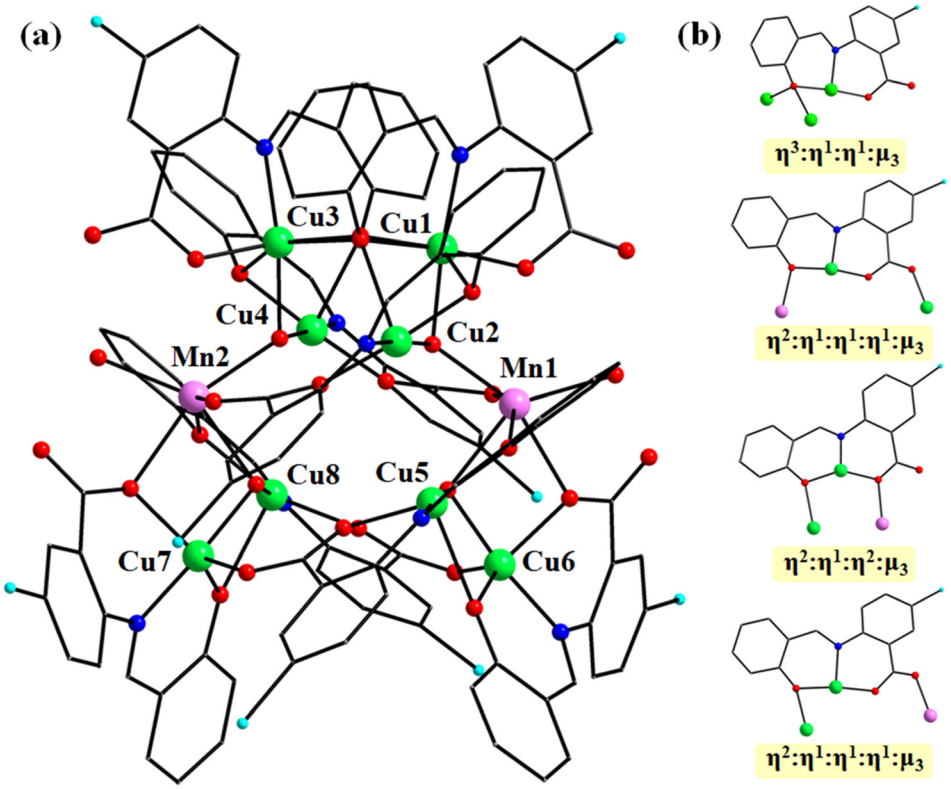

Fig. 4 (a) Partially labeled representation of the molecular structure of **2**, and (b) the crystallographically established coordination modes of all $sacb^{2-}$ ligands present in **2**. All H atoms are omitted for clarity. Color scheme: Cu^{II}, green; Mn^{II}, magenta; O, red; N, blue; C, gray; Cl, cyan.

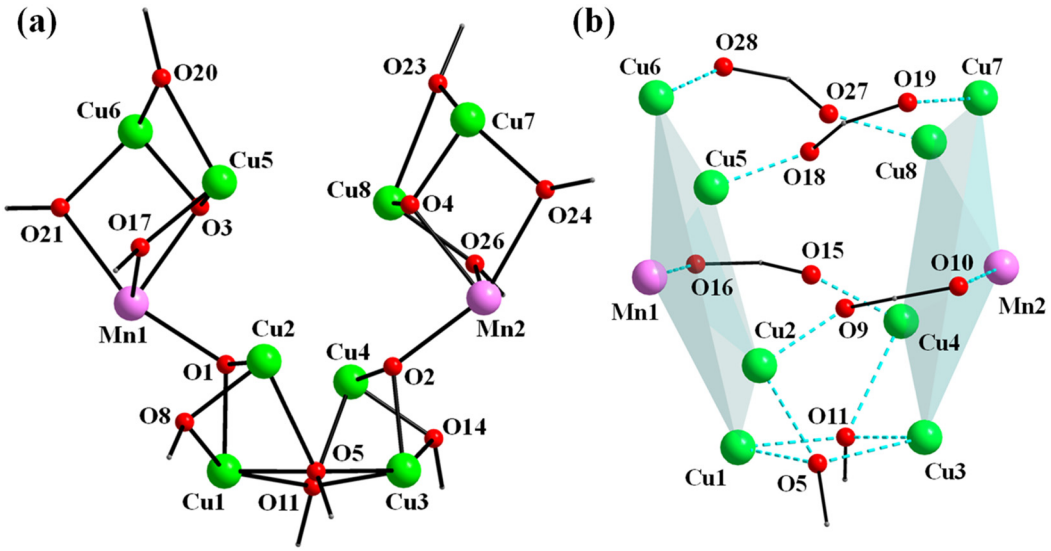

Fig. 5 (a) The complete, labeled $\{Cu_8Mn_2(\mu_3\text{-}OH)_4(\mu\text{-}OR)_6(\mu_3\text{-}OR)_2(\mu\text{-}O_2CR)_2\}^{6+}$ core of **2** and (b) its metal topology, consisting of two pentanuclear $\{Cu_4Mn\}$ units located in opposite sides. The cyan dashed lines indicate the connection of the two subunits *via* eight carboxylate-O and two phenoxo-O atoms of $sacb^{2-}$ ligands. All H atoms are omitted for clarity. The corresponding metal–oxygen–metal bond angles are: Cu1–O1–Mn1 = 121.0(2), Cu2–O1–Cu1 = 92.5(2), Cu2–O1–Mn1 = 119.2(2), Cu3–O2–Cu4 = 94.2(1), Cu3–O2–Mn2 = 117.8(2), Cu4–O2–Mn2 = 123.6(2), Cu5–O3–Cu6 = 104.7(2), Cu5–O3–Mn1 = 106.3(2), Cu6–O3–Mn1 = 103.8(2), Cu7–O4–Mn2 = 106.2(2), Cu8–O4–Cu7 = 103.8(2), Cu8–O4–Mn2 = 103.7(2), Cu1–O5–Cu2 = 80.2(1), Cu5–O17–Mn1 = 102.2(1), Cu6–O20–Cu5 = 89.9(1), Cu6–O21–Mn1 = 96.3(1), Cu7–O24–Mn2 = 98.1(1), and Cu8–O26–Mn2 = 101.0(1). Color scheme: Cu^{II}, green; Mn^{II}, magenta; O, red; C, gray.

coordination modes of the $sacb^{2-}$ ligands are illustrated in Fig. 4b. The ten metal ions are linked through the phenoxo and carboxylate groups of eight doubly deprotonated $sacb^{2-}$ ligands and four μ_3-OH^- groups, affording a $\{Cu_8Mn_2(\mu_3\text{-}OH)_4(\mu\text{-}OR)_6(\mu_3\text{-}OR)_2(\mu\text{-}O_2CR)_2\}^{6+}$ core (Fig. 5a). The core of the compound consists of two pentanuclear $\{Cu_4Mn(\mu_3\text{-}OH)_2(\mu\text{-}OR)_5\}^{3+}$ subunits, each comprising two vertex-sharing $\{Cu_2Mn\}$ triangles, one $\{Cu_2Mn(\mu_3\text{-}OH)(\mu\text{-}OR)_3\}^{2+}$ and one $\{Cu_2Mn(\mu_3\text{-}OH)(\mu\text{-}OR)_2\}^{3+}$ sharing a common Mn atom. The two $\{Cu_4Mn\}$ units are oriented in opposite directions (Fig. 5b) and are linked by four carboxylate and two alkoxido arms of the $sacb^{2-}$ ligands, namely, eight carboxylate-O atoms (O9, O10, O15, O16, O18, O19, O27, O28) and two μ_3-OR^- (O5, O11) bridges. To the best of our knowledge, this type of core structure is unprecedented in heterometallic 3d/3d′-cluster chemistry.

The eight tetradentate $sacb^{2-}$ ligands adopt three coordination modes: $\eta^2{:}\eta^1{:}\eta^1{:}\eta^1{:}\mu_3$ (observed four times), $\eta^3{:}\eta^1{:}\eta^1{:}\mu_3$ (observed twice) and $\eta^2{:}\eta^1{:}\eta^2{:}\mu_3$ (observed twice) (Fig. 4b), acting in all cases as chelating ligands to Cu^{II} atoms *via* their phenoxo-O, imino-N and carboxylate-O atoms. The $\eta^2{:}\eta^1{:}\eta^1{:}\eta^1{:}\mu_3$ and $\eta^2{:}\eta^1{:}\eta^2{:}\mu_3$ $sacb^{2-}$ groups serve as additional bridges to both Cu^{II} and Mn^{II} ions *via* their phenoxo- and carboxylate-O atoms, whereas the $\eta^3{:}\eta^1{:}\eta^1{:}\mu_3$ $sacb^{2-}$ groups exclusively bridge Cu^{II} centers through their phenoxo-O atoms. Each μ_3-OH^- (O1, O2, O3, O4) group further bridges two Cu^{II} ions and one Mn^{II} ion within the four triangular $\{Cu_2Mn\}$ subunits. All four metallic triangles are scalene within the 3σ-criterion (Fig. S3), with Cu···Cu···Mn, Cu···Mn···Cu and Mn···Cu···Cu angles in the range of 61.5–68.1°, 47.0–55.6° and 63.0–67.6°, respectively. The Cu···Cu and Cu···Mn separations span the range 2.858–3.080 and 3.281–3.662 Å, respectively. The coordination spheres of the Mn1 and Mn2 centers are each completed by a terminal H_2O solvate molecule, O29 and O30, respectively.

The coordination geometries of all metal ions in **2** are depicted in Fig. S4. The Cu1, Cu3, Mn1 and Mn2 atoms are six-coordinate adopting distorted octahedral geometries. The coordination geometries of Cu1 and Cu3 are best described as Jahn–Teller distorted octahedral with the two axially elongated bonds formed by phenoxo-O atoms (Cu1–O8 = 2.450(4) Å/Cu1–O11 = 2.468(4) Å/Cu3–O5 = 2.488(4) Å/Cu3–O14 = 2.579(4) Å) of $sacb^{2-}$, while the equatorial planes are occupied by three O,N,O-donor atoms (O5, N1, O6 for Cu1/O11, N3, O12 for Cu3) from $sacb^{2-}$ and a bridging OH^- (O1 for Cu1/O2 for Cu3) group. On the other hand, the Mn1 and Mn2 centers are exclusively bound to six oxygen atoms. Three of them (O16, O17, O21 for Mn1/O10, O24, O26 for Mn2) belong to $sacb^{2-}$ ligands, one (O29 for Mn1/O30 for Mn2) to the terminal H_2O molecule, while the remaining two oxygen atoms belong to bridging OH^- (O1, O3 for Mn1/O2, O4 for Mn2) groups.

The Cu2, Cu4, Cu5 and Cu8 ions are five-coordinate with distorted square pyramidal geometries (τ = 0.13 for Cu2, 0.08 for Cu4, 0.29 for Cu5, and 0.30 for Cu8).[25] The equatorial planes of the Cu^{II} square pyramidal geometries are occupied by three O,N,O-donor atoms (O8, N2, O9 for Cu2/O14, N4, O15 for Cu4/O17, N5, O18 for Cu5/O26, N8, O27 for Cu8) of

$sacb^{2-}$ and one bridging OH^- (O1 for Cu2/O2 for Cu4/O3 for Cu5/O4 for Cu8) group. The apical positions are occupied by phenoxo-O atoms (O5 for Cu2/O11 for Cu4/O20 for Cu5/O5 for Cu8) of $sacb^{2-}$.

The remaining Cu6 and Cu7 atoms are also five-coordinate, but they adopt distorted trigonal bipyramidal geometries (τ = 0.81 for Cu6 and 0.68 for Cu7).[25] The equatorial planes of the Cu^{II} trigonal bipyramidal geometries are occupied by three O-donor atoms (O20, O21, O28 for Cu6/O19, O23, O24 for Cu7) of $sacb^{2-}$, while the axial positions are occupied by one N-donor atom (N6 for Cu6/N7 for Cu7) from $sacb^{2-}$ and one bridging OH^- (O3 for Cu6/O4 for Cu7) group.

The crystal structure of **2** is stabilized by weak intramolecular hydrogen bonding interactions between the terminal H_2O (O29, O30) molecules and the deprotonated, uncoordinated carboxylate-O atoms (O7, O25) of $sacb^{2-}$ ligands, reflected in $O_{H_2O}\cdots O_{sacb}$ distances of 2.696 and 2.699 Å, respectively (Fig. S5a). Additionally, five weak intramolecular $\pi\cdots\pi$ stacking interactions occur between the aromatic rings of $sacb^{2-}$ ligands, with centroid-to-centroid distances ranging from 3.603 to 3.914 Å (Fig. S5b). From a supramolecular standpoint, no significant intermolecular contacts are detected between the decanuclear clusters, implying that the crystallographically independent decanuclear clusters are well-separated in the crystal lattice (Fig. S6). The shortest intermolecular Cu···Cu, Cu···Mn and Mn···Mn distances between adjacent $\{Cu_8Mn_2\}$ clusters in the crystal of **2** are 9.242, 8.924 and 11.282 Å, respectively. The space-filling representation of **2** (Fig. S7) reveals its nanoscale dimensions, with the longest intramolecular Cl···Cl distance being 1.96 nm, excluding hydrogen atoms.

To explore a structural correlation between compounds **1** and **2**, we examined the role of polymer **1** in the formation of

Table 1 To date characterized heterometallic non-polymeric Cu^{II}/Mn^{II} clusters, and their structural and magnetic properties

Complex[a]	Metal topology	Magnetic interactions	Ref.
$[Cu_2Mn(o\text{-}(NO_2)PhCO_2)_2(L1)_2]$[b]	Linear	AF	26
$[Cu_2Mn(o\text{-}(NO_2)PhCO_2)_2(L2)_2]$[c]	Linear	AF	26
$[Cu_2Mn(O_2CMe)_6L_2]$[d]	Linear	AF	27
$[Cu_2Mn(ClO_4)_2L_2(MeOH)_2]$[e]	Triangle	AF	28
$[Cu_2Mn(O_2CMe)_2L_2]$[f]	Linear	AF	29
$[Cu_2Mn(NO_3)_2L_2]$[f]	Linear	AF	29
$[Cu_2Mn(O_2CPh)L_2(H_2O)]Cl$[f]	Triangle	AF	29
$[Cu_2Mn((p\text{-}OH)PhCO_2)L_2(H_2O)]ClO_4$[f]	Triangle	AF	29
$[Cu_2Mn(O_2CH)L_2(H_2O)]ClO_4$[f]	Triangle	AF	29
$[Cu_2Mn(nic)_2L_2]$[f,g]	Linear	AF	9*d*
$[Cu_2MnCl_2(L1)_2]$[h]	Triangle	AF	9*c*
$[Cu_2Mn_2Cl_4(L1)_2]$[h]	Zig-zag	AF	9*c*
$[Cu_2Mn_2(hfac)_2L_2]$[i,j]	Cyclic	F/AF	30
$[Cu_2Mn(O_2CMe)_2(L1)_2]$[b]	Linear	AF	9*f*
$[Cu_2Mn(O_2CCH_2Ph)_2(L1)_2]$[b]	Linear	AF	9*f*
$[Cu_2Mn_3(O_2CPh)_6(L1)_2]$[b]	Linear	AF	9*f*
$[Cu_2Mn_3(m\text{-}(NO_2)PhCO_2)_6(L1)_2]$[b]	Linear	AF	31
$[Cu_2Mn_3(m\text{-}(NO_2)PhCO_2)_6(L2)_2(H_2O)_2]$[c]	Linear	AF	31
$[Cu_2Mn(N_3)_2L_2]$[f]	Triangle	F/AF	32
$[Cu_2Mn(NCO)_2L_2]$[f]	Triangle	F/AF	32
$[Cu_2Mn(NCS)_2L_2]$[f]	Triangle	F/AF	32
$[Cu_3MnL_3(H_2O_2)](ClO_4)_2$[f]	Star-shaped	F/AF	32
$[Cu_3Mn(SCN)_2L_3]$[k]	Star-shaped	AF	33
$[Cu_3Mn(N(CN)_2)_2L_3]$[k]	Star-shaped	AF	33
$[Cu_3MnL_3](ClO_4)_2$[l]	Star-shaped	F	9*b*
$[Cu_2Mn(N(CN)_2)_2(L1)_2]$[h]	Triangle	AF	34
$[Cu_4Mn_2(N(CN)_2)(L1)_4(MeCN)_2](ClO_4)_3$[h]	Two connected triangles	AF	34
$[Cu_2Mn(N_3)_2(L1)_2]$[m]	Triangle	AF	9*h*
$[Cu_2Mn(L3)_2(MeOH)](ClO_4)_2$[n]	Linear	AF	9*g*
$[Cu_2Mn_2(N_3)_2(L2)_2(H_2O)_2](ClO_4)_2$[o]	Zig-zag	F/AF	9*g*
$[Cu_4Mn_5(2pmoap\text{-}2H)_6](NO_3)_6$[p]	Grid	AF	9*e*
$[Cu_8Mn(2pmoap\text{-}2H)_6](NO_3)_6$[p]	Grid	F/AF	9*e*
$[Cu_5Mn_5(edpba)_5(dmso)_7(H_2O)_7]$[q]	Cyclic	F/AF	9*a*
$[Cu_8Mn_2(OH)_4(sacb)_8(H_2O)_2]$	Four connected triangles	AF	t.w.

[a] Lattice solvate molecules have been omitted. Ligand abbreviations. [b] $L1H_2$ = *N*,*N*′-bis(2-hydroxynaphthyl-methylidene)-1,3-propanediamine. [c] $L2H_2$ = *N*,*N*′-bis(methyl-2-hydroxynaphthyl-methylidene)-1,3-propanediamine. [d] L = 2-*tert*-butyl-5-(2-pyridyl)-2*H*-tetrazole. [e] LH_2 = 2,2′-((1*E*,1′*E*)-(cyclohexane-1,2-diylbis(azanylylidene))bis(methanylylidene))diphenol. [f] LH_2 = *N*,*N*′-bis(α-methylsalicylidene)-1,3-propanediamine. [g] nicH = nicotinic acid. [h] $L1H_2$ = *N*-(α-methylsalicylidene)-*N*′-(salicylidene)-1,3-propanediamine. [i] LH_3 = 1-(2-hydroxybenzamido)-2-((2-hydroxy-3-methoxybenzylidene)amino)ethane. [j] hfacH = hexafluoroacetylacetone. [k] LH_2 = 2,3-dioxo-5,6:15,16-dibenzo-1,4,8,13-tetraazacyclotetradeca-7,13-diene. [l] LH_2 = *N*,*N*′-bis(salicylidene)-1,4-butanediamine. [m] LH_2 = *N*-(α-methylsalicylidene)-*N*′-(salicylidene)-2,2-dimethyl-1,3-propanediamine. [n] $L3H_2$ = *N*,*N*′-cyclohexane-bis(3-ethoxysalicylaldiimine). [o] $L2H_2$ = *N*,*N*′-ethylene-bis(3-ethoxysalicylaldiimine). [p] $2pmoapH_2$ = (2*Z*,2′*Z*)-*N*′,*N*″-(pyridine-2,6-dicarbonyl)bis(pyrimidine-2-carbohydrazonamide). [q] $edpbaH_4$ = *N*,*N*′-2,2′-ethylenediphenylenebis(oxamic acid); AF = antiferromagnetic; F = ferromagnetic; t.w. = this work.

cluster **2**. A $\{Cu_2(sacb)_2\}$ fragment, which is a part of the repeating unit of **1**, is also present in **2** and may serve as a structural 'starting point'. Two key differences are evident in this fragment: (i) the absence of a terminal MeOH molecule from **1**, and (ii) the conversion of two μ-OR^- in **1** into two μ_3-OR^- bridges in **2**. Each μ_3-OR^- group provides further bridging to an additional Cu^{II} center. These observations suggest that nucleation of **2** proceeds "vertically" (top-to-bottom) *via* self-assembly, as illustrated in Fig. S8.

Given the scarcity of previously reported non-polymeric Mn^{II}/Cu^{II} heterometallic clusters, we have compiled them in Table 1 to allow convenient comparison of their nuclearities, metal core topologies, and pertinent magnetic data, such as the nature of predominant magnetic exchange interactions. Inspection of Table 1 shows that the great majority are trinuclear species with either linear or triangular metal topologies and tetranuclear complexes exhibiting zig-zag, cyclic or star-shaped metallic cores,[9b–d,9f–h,26–29,32–34] with considerably fewer pentanuclear examples (linear),[9f,31] a single hexanuclear case (two connected triangles),[34] and two enneanuclear "grid"-like species.[9e] In most Mn^{II}/Cu^{II} compounds the magnetic exchange is predominantly antiferromagnetic (AF) or a combination of ferromagnetic and antiferromagnetic interactions (F/AF), most commonly mediated through phenoxido/alkoxido bridges *via* efficient overlap of nearly collinear magnetic orbitals. Triangular and related motifs frequently host competing interactions that reduce the total spin ground state. Pure ferromagnetic coupling is rare and appears only in the star-shaped tetranuclear complex $[Cu_3MnL_3](ClO_4)_2$ that features a salen-type Schiff base ligand (LH_2).[9b] Finally, it is noteworthy that complex **2**, together with the heterometallic wheel $[Cu_5Mn_5(edpba)_5(dmso)_7(H_2O)_7]$ that incorporates the flexible bis-oxamate $edpbaH_4$ ligand, represent the highest nuclearity reported to date for Mn^{II}/Cu^{II} compounds. The latter decanuclear wheel displays relatively strong antiferromagnetic interactions between the Cu^{II} and Mn^{II} centers, resulting in a spin ground state of S = 10 from an overall ferrimagnetic behavior.[9a]

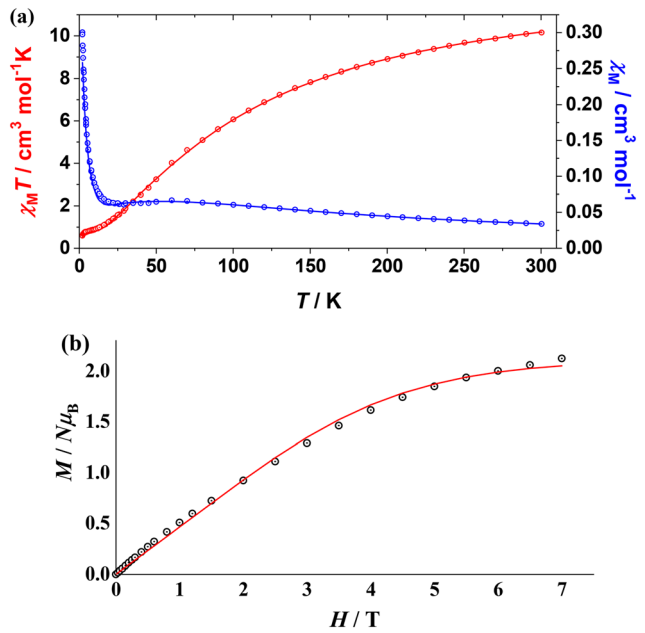

Fig. 6 (a) Plots of $\chi_M T$ *vs.* T and χ_M *vs.* T for complex **2** in a 0.1 T dc field; the solid lines are the best-fit curves (see text for details). (b) Plot of magnetization (M) *vs.* field (H) for complex **2** at 2 K; the solid line is the best-fit curve.

c. Magnetic studies

The magnetic characterization of **2** is noteworthy because, to the best of our knowledge, no prior magnetic studies have been carried out on a crystal structure with such a metal core-topology. Direct current (dc) magnetic susceptibility (χ_M) measurements were performed on an analytically pure microcrystalline sample of **2** over 2–300 K under an applied static magnetic field of 0.1 T. The data are presented as $\chi_M T$ (red, left axis) and χ_M (blue, right axis) *vs.* T in Fig. 6a. At 300 K, the $\chi_M T$ value of compound **2** is 10.16 cm^3 mol^{-1} K, lower than the spin only value expected for two S = 5/2 Mn^{II} and eight S = 1/2 Cu^{II} non-interacting spin carriers (11.75 cm^3 mol^{-1} K for g = 2.00), suggesting that antiferromagnetic exchange interactions dominate even at room temperature. Upon cooling, $\chi_M T$ decreases steeply from 300 to ~50 K and then more gradually, showing a shallow plateau near 0.8 cm^3 mol^{-1} K before falling to 0.30 cm^3 mol^{-1} K at 2 K. The shape of the $\chi_M T$ *vs.* T plot suggests the presence of predominant intramolecular Cu···Mn and Cu···Cu antiferromagnetic exchange interactions let alone single ion effects, such as zero field splitting, and/or Zeeman contributions. In addition, the monotonic increase of χ_M on cooling with a progressively steeper increase towards low temperatures and no peak or downturn indicates the absence of long-range ordering above 2 K and dominant antiferromagnetic exchange, leading to a small ground state spin value.

The field dependent magnetization of complex **2** at 2 K (Fig. 6b) reveals a relatively rapid increase up to a quasi-saturated value of 2.05$N\mu_B$ under an applied field of 7 T. This value is significantly lower than the theoretical maximum value of 18.00$N\mu_B$ ($M/N\mu_B = n_{Cu}{\cdot}g_{Cu}{\cdot}S_{Cu} + n_{Mn}{\cdot}g_{Mn}{\cdot}S_{Mn}$), expected for eight ($n$ = 8) Cu^{II} (S = 1/2, g = 2) and two (n = 2) Mn^{II} (S = 5/2, g = 2) ions. The low temperature $\chi_M T$ and the high field magnetization values evidence antiferromagnetic exchange interactions and an overall ground state spin value of S = 1.

The susceptibility and magnetization data of compound **2** were fit using PHI program,[35] to evaluate the nature and magnitude of the intramolecular Cu···Mn and Cu···Cu magnetic exchange interactions. The structural data of **2** show multiple bridging ligation within the $\{Cu_8Mn_2\}$ metallic core. Excluding the axially elongated Cu–O bonds, the complex can be magnetically envisaged as two $\{Cu_4Mn\}$ units,

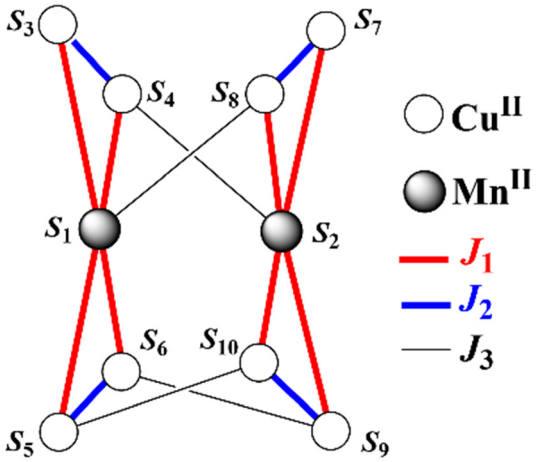

Fig. 7 *J*-Coupling scheme employed for the elucidation of the magnetic exchange interactions in complex **2**.

each comprising two vertex-sharing {Cu_2Mn} triangles that are connected by four *syn–anti* carboxylate bridges from $sacb^{2-}$ ligands. To avoid overparameterization, assuming similar magnetic interactions for all the Mn^{II}–O–Cu^{II} contacts and for the *syn–anti* carboxylate superexchange pathways, the magnetic system was modelled with three isotropic exchange coupling constants (Fig. 7): J_1 for the eight $Mn^{II}\cdots Cu^{II}$ interactions, J_2 for the four $Cu^{II}\cdots Cu^{II}$ interactions, and J_3 for the *syn–anti* carboxylate-induced contacts. Therefore, the spin Hamiltonian used for this system is represented by the following eqn (3):

$$\hat{H} = -2J_1(S_1\cdot S_3 + S_1\cdot S_4 + S_1\cdot S_5 + S_1\cdot S_6 + S_2\cdot S_7 + S_2\cdot S_8 + S_2\cdot S_9 + S_2\cdot S_{10}) - 2J_2(S_3\cdot S_4 + S_5\cdot S_6 + S_7\cdot S_8 + S_9\cdot S_{10}) - 2J_3(S_1\cdot S_8 + S_2\cdot S_4 + S_5\cdot S_{10} + S_6\cdot S_9) \quad (3)$$

The best-fit parameters from the simultaneous susceptibility and magnetization data were: J_1 = −16.5(1) cm^{-1}, J_2 = −35.1(5) cm^{-1}, J_3 = +0.7(3) cm^{-1} and g = 2.114(2). Attempts to distinguish inequivalent Cu⋯Mn and Cu⋯Cu pathways led to overparametrization without improving the fit. The magnitude and sign of the obtained J values are consistent with moderate antiferromagnetic superexchange interactions through M–O–M angles around or above 100° (J_1 and J_2) and a very weak ferromagnetic contribution for the *syn–anti* carboxylate bridges (J_3). The extracted J values are in good agreement with previously reported exchange parameters for various Mn^{II}–Cu^{II} systems.[9c,d,f]

The energy level analysis of the spin levels of **2** indicates quasi degenerate S = 0 and S = 1 ground spin states, which account for the intermediate low temperature $\chi_M T$ value (between 0 and 1), and the quasi saturation of magnetization value at 7 T ($2.05N\mu_B$). The first excited spin manifold lies ~45 cm^{-1} above the ground state and explains the shallow maximum/plateau in $\chi_M T$ near 50 K. As expected, complex **2** did not exhibit any SMM behavior, either in the absence or presence of an external dc field, indicating the absence of magnetization relaxation.

4. Concluding comments and perspectives

In summary, we demonstrated that the preformed 1-D helical chain $[Cu^{II}_2(sacb)_2(MeOH)]_n$ (**1**) serves as an effective building block for the one-pot assembly of the new decanuclear 0-D heterometallic cluster $[Cu^{II}_8Mn^{II}_2(OH)_4(sacb)_8(H_2O)_2]$ (**2**), using a second 3d′-metal source. These are the first homometallic Cu^{II} and heterometallic 3d/3d′ complexes incorporating the chelating/bridging Schiff base ligand $sacbH_2$. Structural analysis reveals that complex **2** features a unique metal core topology consisting of two oppositely aligned, {Cu_4Mn} units, each comprising two vertex-sharing $\{Cu_2Mn(\mu_3\text{-}OH)\}^{5+}$ triangles, connected by four carboxylate and two phenoxo groups from the $sacb^{2-}$ chelates. This compound also represents one of the two highest nuclearity Mn^{II}/Cu^{II} clusters reported to date. Compound **1** appears to direct the assembly of **2**, as they both share the {$Cu_2(sacb)_2$} fragment, which likely serves as a nucleation site. Magnetically, complex **2** exhibits predominantly antiferromagnetic exchange interactions between the Cu⋯Mn and Cu⋯Cu pairs, quantitively described by the coupling constants J_1 = −16.5(1) cm^{-1} and J_2 = −35.1(5) cm^{-1}, respectively.

Building on these results, we are currently trying to expand this synthetic route to access new heterometallic 3d/3d′ compounds bearing $sacbH_2$ chelate, as well as other similar Schiff bases, as this chemistry remains largely unexplored. In particular, targeted substitution of isotropic Mn^{II} ions by anisotropic Co^{II} within the {Cu_8Mn_2} cluster is expected to enhance the overall magnetic anisotropy and maybe 'switch-on' the SMM behavior. Parallel efforts explore additional 3d/3d′ combinations, including Cu^{II}–Fe^{III}, Ni^{II}–Fe^{III}, Co^{II}–Fe^{III} and Ni^{II}–$Mn^{II/III/IV}$, to probe the structural architectures and the magnetic properties of the resulting compounds.

Conflicts of interest

The authors declare no competing financial interest.

Data availability

All crystallographic data supporting the findings of this study have been deposited with the Cambridge Crystallographic Data Centre (CCDC).

Additional experimental data, including synthetic procedures, spectroscopic characterisation, magnetic measurements, and supplementary figures, are included in the supplementary information (SI) associated with this article. Further datasets generated or analysed during the current study are available from the corresponding author upon reasonable request.

Supplementary information is available. See DOI: https://doi.org/10.1039/d5ce01110h.

CCDC 2504835 and 2504836 contain the supplementary crystallographic data for this paper.[36a,b]

Acknowledgements

This work has been supported by the funding program "MEDICUS" of the University of Patras (to D. I. A.). A. E. thanks MICIU, project PID2023-146166NB-I00 for supporting this work.

Notes and references

1 (*a*) C. L. Hill and C. M. Prosser-McCartha, *Coord. Chem. Rev.*, 1995, **143**, 407–455; (*b*) S. Mukherjee, J. A. Stull, J. Yano, Th. C. Stamatatos, K. Pringouri, T. A. Stich, K. A. Abboud, R. D. Britt, V. Yachandra and G. Christou, *Proc. Natl. Acad. Sci. U. S. A.*, 2012, **109**, 2257–2262; (*c*) D. Gatteschi and R. Sessoli, *Angew. Chem., Int. Ed.*, 2003, **42**, 268–297; (*d*) C. C. Beedle, C. J. Stephenson, K. J. Heroux, W. Wernsdorfer and D. N. Hendrickson, *Inorg. Chem.*, 2008, **47**, 10798–10800.

2 Y.-K. Deng, H.-F. Su, J.-H. Xu, W.-G. Wang, M. Kurmoo, S.-C. Lin, Y.-Z. Tan, J. Jia, D. Sun and L.-S. Zheng, *J. Am. Chem. Soc.*, 2016, **138**, 1328–1334.

3 (*a*) C. Papatriantafyllopoulou, E. E. Moushi, G. Christou and A. J. Tasiopoulos, *Chem. Soc. Rev.*, 2016, **45**, 1597–1628; (*b*) R. Sessoli, D. Gatteschi and J. Villain, in *Molecular Nanomagnets*, Oxford University Press, Oxford, UK, 2006.

4 (*a*) L. Bogani and W. Wernsdorfer, *Nat. Mater.*, 2008, **7**, 179–186; (*b*) R. Vincent, S. Klyatskaya, M. Ruben, W. Wernsdorfer and F. Balestro, *Nature*, 2012, **488**, 357–360; (*c*) M. Urdampilleta, S. Klyatskaya, J.-P. Cleuziou, M. Ruben and W. Wernsdorfer, *Nat. Mater.*, 2011, **10**, 502–506.

5 (*a*) R. Sessoli, H. Tsai, A. R. Schake, S. Wang, J. Vincent, K. Folting, D. Gatteschi, G. Christou and D. N. Hendrickson, *J. Am. Chem. Soc.*, 1993, **115**, 1804–1816; (*b*) R. Bagai and G. Christou, *Chem. Soc. Rev.*, 2009, **38**, 1011–1026.

6 C. J. Milios, A. Vinslava, W. Wernsdorfer, S. Moggach, S. Parsons, S. P. Perlepes, G. Christou and E. K. Brechin, *J. Am. Chem. Soc.*, 2007, **129**, 2754–2755.

7 (*a*) K. Liu, W. Shi and P. Cheng, *Coord. Chem. Rev.*, 2015, **289–290**, 74–122; (*b*) Vipanchi, K. R. Vignesh, A. S. Armenis, D. I. Alexandropoulos and Th. C. Stamatatos, *ChemPhysChem*, 2024, **25**, e202400385.

8 (*a*) A. Das, K. Gieb, Y. Krupskaya, S. Demeshko, S. Dechert, R. Klingeler, V. Kataev, B. Büchner, P. Müller and F. Meyer, *J. Am. Chem. Soc.*, 2011, **133**, 3433–3443; (*b*) C. Plenk, T. Weyhermüller and E. Rentschler, *Chem. Commun.*, 2014, **50**, 3871–3873; (*c*) M. Charalambous, E. E. Moushi, T. N. Nguyen, C. Papatriantafyllopoulou, V. Nastopoulos, G. Christou and A. J. Tasiopoulos, *Front. Chem.*, 2019, **7**, 96; (*d*) D. I. Alexandropoulos, M. J. Manos, C. Papatriantafyllopoulou, S. Mukherjee, A. J. Tasiopoulos, S. P. Perlepes, G. Christou and Th. C. Stamatatos, *Dalton Trans.*, 2012, **41**, 4744–4747.

9 (*a*) W. D. Do Pim, E. N. De Faria, W. X. C. Oliveira, C. B. Pinheiro, W. C. Nunes, J. Cano, F. Lloret, M. Julve, H. O. Stumpf and C. L. M. Pereira, *Dalton Trans.*, 2015, **44**, 10939–10942; (*b*) S. Mondal, S. Mandal, L. Carrella, A. Jana, M. Fleck, A. Köhn, E. Rentschler and S. Mohanta, *Inorg. Chem.*, 2015, **54**, 117–131; (*c*) P. Mahapatra, S. Giri, M. G. B. Drew and A. Ghosh, *Dalton Trans.*, 2018, **47**, 3568–3579; (*d*) S. Dutta, T. K. Ghosh, P. Mahapatra and A. Ghosh, *Inorg. Chem.*, 2020, **59**, 14989–15003; (*e*) L. N. Dawe, K. V. Shuvaev and L. K. Thompson, *Inorg. Chem.*, 2009, **48**, 3323–3341; (*f*) S. Ganguly, J. Mayans and A. Ghosh, *Chem. – Asian J.*, 2020, **15**, 4055–4069; (*g*) E. Pilichos, M. Font-Bardia, A. Escuer and J. Mayans, *Dalton Trans.*, 2022, **51**, 17653–17663; (*h*) E. Pilichos, P. Bhunia, M. Font-Bardia, A. Ghosh, J. Mayans and A. Escuer, *Dalton Trans.*, 2022, **51**, 1779–1783.

10 (*a*) V. A. Milway, F. Tuna, A. R. Farrell, L. E. Sharp, S. Parsons and M. Murrie, *Angew. Chem., Int. Ed.*, 2013, **52**, 1949–1952; (*b*) W.-G. Wang, A.-J. Zhou, W.-X. Zhang, M.-L. Tong, X.-M. Chen, M. Nakano, C. C. Beedle and D. N. Hendrickson, *J. Am. Chem. Soc.*, 2007, **129**, 1014–1015; (*c*) Z. Peng, S. Li, A. Li, J. Liao, Y. Wang, X. Li, W. Meng and J. Zhang, *Dalton Trans.*, 2022, **51**, 2652–2655; (*d*) S. Yamashita, T. Shiga, M. Kurashina, M. Nihei, H. Nojiri, H. Sawa, T. Kakiuchi and H. Oshio, *Inorg. Chem.*, 2007, **46**, 3810–3812; (*e*) J. M. Frost, F. J. Kettles, C. Wilson and M. Murrie, *Dalton Trans.*, 2016, **45**, 18094–18097.

11 (*a*) C. Duboc, *Chem. Soc. Rev.*, 2016, **45**, 5834–5847; (*b*) T. J. Pearson, M. S. Fataftah and D. E. Freedman, *Chem. Commun.*, 2016, **52**, 11394–11397; (*c*) T. T. Da Cunha, V. M. M. Barbosa, W. X. C. Oliveira, E. F. Pedroso, D. M. A. García, W. C. Nunes and C. L. M. Pereira, *Inorg. Chem.*, 2020, **59**, 12983–12987; (*d*) K. Uchida, G. Cosquer, K. Sugisaki, H. Matsuoka, K. Sato, B. K. Breedlove and M. Yamashita, *Dalton Trans.*, 2019, **48**, 12023–12030.

12 (*a*) C. P. Landee and M. M. Turnbull, *Eur. J. Inorg. Chem.*, 2013, 2266–2285; (*b*) A. Borta, E. Jeanneau, Y. Chumakov, D. Luneau, L. Ungur, L. F. Chibotaru and W. Wernsdorfer, *New J. Chem.*, 2011, **35**, 1270–1279.

13 (*a*) P. Bhunia, S. Maity, T. K. Ghosh, A. Mondal, J. Mayans and A. Ghosh, *Dalton Trans.*, 2024, **53**, 9171–9182; (*b*) S. Maity, P. Bhunia, K. Ichihashi, T. Ishida and A. Ghosh, *New J. Chem.*, 2020, **44**, 6197–6205.

14 (*a*) E. C. Mazarakioti, J. Regier, L. Cunha-Silva, W. Wernsdorfer, M. Pilkington, J. Tang and Th. C. Stamatatos, *Inorg. Chem.*, 2017, **56**, 3568–3578; (*b*) K. N. Pantelis, G. Karotsis, C. Lampropoulos, L. Cunha-Silva, A. Escuer and Th. C. Stamatatos, *Materials*, 2020, **13**, 1352; (*c*) A. A. Athanasopoulou, C. P. Raptopoulou, A. Escuer and Th. C. Stamatatos, *RSC Adv.*, 2014, **4**, 12680–12684; (*d*) A. A. Athanasopoulou, M. Pilkington, C. P. Raptopoulou, A. Escuer and Th. C. Stamatatos, *Chem. Commun.*, 2014, **50**, 14942–14945; (*e*) P. S. Perlepe, A. A. Athanasopoulou, K. I. Alexopoulou, C. P. Raptopoulou, V. Psycharis, A. Escuer, S. P. Perlepes and Th. C. Stamatatos, *Dalton Trans.*, 2014, **43**, 16605–16609; (*f*) K. N. Pantelis, K. H. Baka, L. Cunha-Silva, J. Tang, D. I. Alexandropoulos and Th. C. Stamatatos, *Cryst. Growth Des.*, 2025, **25**, 4553–4564.

15 K. N. Pantelis, S. G. Skiadas, Z. G. Lada, R. Clérac, Y. Sanakis, P. Dechambenoit and S. P. Perlepes, *New J. Chem.*, 2024, **48**, 11221–11232.

16 G. A. Bain and J. F. Berry, *J. Chem. Educ.*, 2008, **85**, 532–536.
17 T. Kottke and D. Stalke, *J. Appl. Crystallogr.*, 1993, **26**, 615–619.
18 L. Palatinus and G. Chapuis, *J. Appl. Crystallogr.*, 2007, **40**, 786–790.
19 G. M. Sheldrick, *Acta Crystallogr., Sect. C: Struct. Chem.*, 2015, **71**, 3–8.
20 O. V. Dolomanov, L. J. Bourhis, R. J. Gildea, J. A. K. Howard and H. Puschmann, *J. Appl. Crystallogr.*, 2009, **42**, 339–341.
21 K. Brandenburg, *DIAMOND, Release 3. 1f*, Crystal Impact GbR, Bonn, Germany, 2008, p. 389.
22 I. J. Bruno, J. C. Cole, P. R. Edgington, M. K. Kessler, C. F. Macrae, P. McCabe, J. Pearson and R. Taylor, MERCURY, *Acta Crystallogr., Sect. B: Struct. Sci.*, 2002, **58**, 389–397.
23 K. Nakamoto, *Infrared and Raman Spectra of Inorganic and Coordination Compounds*, Wiley, New York, USA, 4th edn, 1986.
24 W. Liu and H. H. Thorp, *Inorg. Chem.*, 1993, **32**, 4102–4105.
25 A. W. Addison, T. N. Rao, J. Reedijk, J. van Rijn and G. C. Verschoor, *J. Chem. Soc., Dalton Trans.*, 1984, 1349–1356.
26 S. Ganguly, P. Bhunia, J. Mayans and A. Ghosh, *Inorg. Chim. Acta*, 2023, **549**, 121404.
27 A. P. Mosalkova, S. V. Voitekhovich, A. S. Lyakhov, L. S. Ivashkevich, J. Lach, B. Kersting, P. N. Gaponik and O. A. Ivashkevich, *Dalton Trans.*, 2013, **42**, 2985–2997.
28 N. Hari, S. Mandal, A. Jana, H. A. Sparkes and S. Mohanta, *RSC Adv.*, 2018, **8**, 7315–7329.
29 S. Dutta, P. Bhunia, J. Mayans, M. G. B. Drew and A. Ghosh, *Dalton Trans.*, 2020, **49**, 11268–11281.
30 S. Osa, Y. Sunatsuki, Y. Yamamoto, M. Nakamura, T. Shimamoto, N. Matsumoto and N. Re, *Inorg. Chem.*, 2003, **42**, 5507–5512.
31 S. Ganguly, P. Bhunia, J. Mayans and A. Ghosh, *New J. Chem.*, 2022, **46**, 17260–17271.
32 S. Biswas, S. Naiya, C. J. Gómez-García and A. Ghosh, *Dalton Trans.*, 2012, **41**, 462–473.
33 S. Wang, G. Yang, R. Li, Y. Wang and D. Liao, *Eur. J. Inorg. Chem.*, 2004, 4907–4913.
34 P. Mahapatra, M. G. B. Drew and A. Ghosh, *Cryst. Growth Des.*, 2017, **17**, 6809–6820.
35 N. F. Chilton, R. P. Anderson, L. D. Turner, A. Soncini and K. S. Murray, *J. Comput. Chem.*, 2013, **34**, 1164–1175.
36 (*a*) CCDC 2504835: Experimental Crystal Structure Determination, 2025, DOI: 10.5517/ccdc.csd.cc2q2h4g; (*b*) CCDC 2504836: Experimental Crystal Structure Determination, 2025, DOI: 10.5517/ccdc.csd.cc2q2h5h.